Journal of Solid State Chemistry 237 (2016) 64–71

Contents lists available at ScienceDirect

Journal of Solid State Chemistry

journal homepage: www.elsevier.com/locate/jssc

New ferroelastic $K_2Sr(MoO_4)_2$: Synthesis, phase transitions, crystal and domain structures, ionic conductivity

Galina D. Tsyrenova [a,b], Erzhena T. Pavlova [b], Sergey F. Solodovnikov [c,d], Nadezhda N. Popova [a,c], Tatyana Yu. Kardash [e], Sergey Yu. Stefanovich [f], Irina A. Gudkova [c], Zoya A. Solodovnikova [c], Bogdan I. Lazoryak [f,*]

[a] Baikal Institute of Nature Management, Siberian Branch, Russian Academy of Sciences, Sakh'yanova St. 6, Ulan-Ude, 670047 Buryat Republic, Russia
[b] Buryat State University, Smolin St. 24a, Ulan-Ude, 670000 Buryat Republic, Russia
[c] Nikolaev Institute of Inorganic Chemistry, Siberian Branch, Russian Academy of Sciences, Acad. Lavrentyev Ave. 3, Novosibirsk 630090, Russia
[d] Novosibirsk State University, Pirogov St. 2, Novosibirsk 630090, Russia
[e] Boreskov Institute of Catalysis, Siberian Branch, Russian Academy of Sciences, Acad. Lavrentiev Ave. 5, Novosibirsk 630090, Russia
[f] Department of Chemistry, Moscow State University, 119899 Moscow, Russia

ARTICLE INFO

Article history:
Received 19 November 2015
Received in revised form
17 January 2016
Accepted 18 January 2016
Available online 19 January 2016

Keywords:
Potassium
Strontium
molybdates
Phase transitions
Ferroelastics
Crystal structure
Crystal optics analysis
Domain structure
Ionic conductivity

ABSTRACT

$K_2Sr(MoO_4)_2$ crystals were synthesized and their properties examined. The distortive polymorphic transformations at 421 K (α (LT)→ β(MT)) and 744 K (β(MT)→γ (HT)) of $K_2Sr(MoO_4)_2$ were studied. It has been shown that the transitions go in sequence from the high-temperature palmierite $K_2Pb(SO_4)_2$-type γ-phase ($R\bar{3}m$) to an intermediate β-phase with a probable incommensurate structure and then to a low-temperature α-phase. Domain structures peculiarities in ferroelastic α-$K_2Sr(MoO_4)_2$ have been investigated. The electrical conductivity of $K_2Sr(MoO_4)_2$ rises tenfold in the vicinity of the phase transition at 744 K that may be associated with a change conductivity path from quasi-one-dimensional to two-dimensional. The crystal structure of the α-phase (sp. gr. $C2/c$, $a=14.318(3)$ Å, $b=5.9337(12)$ Å, $c=10.422(2)$ Å, $\beta=105.83(3)^\circ$, $Z=4$, $R=0.0219$) is similar to that of α-$Pb_3(PO_4)_2$. Sr-atoms are mainly located at site with the coordination number CN=8 (a tetragonal antiprism with bond lengths of 2.578(2)–2.789(2) Å) and K atoms are located at site with CN=9+1.

1. Introduction

Investigation of a wide variety of active dielectric crystals and ferroelastics, and the development of their preparation methods has opened the way to fundamentally new types of acoustoelectric devices, optic shutters and keys, logic and memory elements, displays, etc. Applications of ferroelastics are based on their switchable crystal orientations and the control of their domain structures through small mechanical and thermal deformations [1]. At present, the mechanism of formation and switching of domains in ferroelastics is not studied enough. Therefore, further studies of domain structures transformation depending on temperature in new crystals are needed.

A promising group of ferroelastics with tetrahedral XO_4 anions is presented by a large family of compounds with formulae $M_3(XO_4)_2$ (M=Sr, Ba, Pb; X=P, As, V, Cr), $A_2M(XO_4)_2$ (A=K, Rb, Cs, Tl; M=Sr, Ba, Pb; X=S, Se, Cr, Mo, W), $A_5R(MoO_4)_4$ (A=K, Rb, Tl; R=RE, Y, Bi, Fe, In), etc. [2–4]. In their paraelastic phases they are isotypic with the trigonal palmierite $K_2Pb(SO_4)_2$ (sp. gr. $R\bar{3}m$; $a=5.50$ Å; $c=20.86$ Å) [5]. The crystal chemical formula of the palmierite-type structure is $M1^{[6+6]}M2_2^{[9+1]}(XO_4)_2$. The best known representatives of the family are monoclinic ferroelastics $Pb_3(XO_4)_2$ (X=P, As, V). The ferroelastic transition $R\bar{3}m \rightarrow C2/c$ at 453 K in $Pb_3(PO_4)_2$ is mainly realized through shifts of the Pb^{2+} cations and PO_4^{3-} anions from the threefold axes [6,7]. The monoclinic $Pb_3(PO_4)_2$ cell vectors of the ferroelastic phase, $\boldsymbol{a}_m$, $\boldsymbol{b}_m$, $\boldsymbol{c}_m$, and the trigonal paraphase cell vectors, $\boldsymbol{a}_t$, $\boldsymbol{b}_t$, $\boldsymbol{c}_t$, are related by the expressions $\boldsymbol{a}_m=-2/3\boldsymbol{a}_t - 1/3\boldsymbol{b}_t+2/3\boldsymbol{c}_t$; $\boldsymbol{b}_m=-\boldsymbol{b}_t$; $\boldsymbol{c}_m=2\boldsymbol{a}_t+\boldsymbol{b}_t$ [7]. Ferroelastic second-order transitions from the trigonal phase to the monoclinic one were also found in $K_2Pb(MoO_4)_2$, $Rb_2Pb(MoO_4)_2$, and $Cs_2Pb(MoO_4)_2$, at 448, 496, and 626 K, respectively [8]. The existence of the phase transitions in those compounds is attributed to the effect of $6s^2$ lone electron pairs of Pb^{2+} [3]. The crystal structures of monoclinic $K_2Pb(MoO_4)_2$ [9] and $Rb_2Pb(MoO_4)_2$ [10] show a different

* Corresponding author.
E-mail address: bilazoryak@gmail.com (B.I. Lazoryak).

http://dx.doi.org/10.1016/j.jssc.2016.01.011
0022-4596/

character of the distortion of the palmierite structure in comparison with the structure $Pb_3(PO_4)_2$.

Double molybdate $K_2Sr(MoO_4)_2$ [11] has the palmierite-like structure as well. However, information about the crystal symmetry of $K_2Sr(MoO_4)_2$ is controversial. $K_2Sr(MoO_4)_2$ was reported to crystallize in sp. gr. $C2/m$ with the lattice parameters $a=10.42$ Å, $b=5.929$ Å, $c=7.606$ Å; $\beta=115°19'$; $Z=2$ [11], while this compound was also described as a trigonal system with the parameters of $a_{hex}=5.973$ Å, $c_{hex}=20.63$ Å [2].

In this work, we report on the synthesis of single crystals and powder of $K_2Sr(MoO_4)_2$ detailed crystallographic characterization by X-ray diffraction, phase transitions and domain structure investigations of lamellar crystals of this compound.

2. Experimental section

2.1. Synthesis

$K_2Sr(MoO_4)_2$ powder was prepared by a conventional solid state method from a stoichiometric mixture of chemically pure K_2CO_3, $SrCO_3$ and MoO_3 at 573–923 K for 80 h. Transparent colorless lamellar crystals of $K_2Sr(MoO_4)_2$ suitable for X-ray structure and optical studies were obtained by a spontaneous flux crystallization from a melt of the composition 56 mol% K_2MoO_4 +20 mol% $SrMoO_4$+24 mol% MoO_3 in the 1053–703 K range with the cooling rate of 3 K h^{-1}.

2.2. Characterization

The identification of the compound was performed by powder X-ray diffraction (XRD) on a D8 Advance Bruker AXS GmbH diffractometer with Bragg-Brentano geometry (CuK_α radiation, $2\theta=5$–$70°$, scanning step 0.02°).

X-ray powder diffraction (XRD) measurements were performed at 298, 573, and 773 K on diffractometer (CuK_α radiation) with a parallel X-ray beam geometry produced by a parabolic Göbel mirror, a graphite crystal analyzer and a scintillation detector. Samples were heated in a high-temperature Anton Paar HTK-16 chamber with a Pt heater as a holder. XRD patterns were registered in the 2θ range of 10–70° with 0.02° step; they were indexed by the TOPAS program v.4.2 [12]. The cell parameters obtained were used in the Le Bail fitting.

The differential scanning calorimetric (DSC) analysis of the samples was carried out on a NETZCH DSC 204 thermal analyzer upon heating at 10.0 K/min.

Single-crystal X-ray data were collected with a Bruker Nonius X8 Apex CCD diffractometer at room temperature using a standard procedure (MoK_α radiation, graphite monochromator, φ-scanning with a step $\Delta\varphi=0.5°$). The structure was solved and refined with the SHELX97 program package [13].

The electrical conduction (σ) dielectric permeability (ε) and dielectric loss tangent ($tg\delta$) were measured on a Novocontrol Beta-N impedance-analyzer in a ProboStat measuring cell using the double-contact method [14] in the frequency range of 0.3 Hz to 1 MHz on heating at 353–873 K with 2 K min^{-1}; ceramic pellets were 10.15 mm in diameter and 2.43 mm in height.

The second harmonic generation (SHG) response of powder samples was measured with a Q-switched YAG:Nd laser at $\lambda_\omega=1064$ nm, in the reflection mode. Intensities of the SHG signal ($I_{2\omega}$) from the sample and those from a reference sample (polycrystalline α-SiO_2) were recorded.

Crystal optical observations were performed on a POLAM-211C polarizing microscope equipped with a hot stage in the range of 300–973 K with ±5 K accuracy. The crystal sample was placed into a platinum loop heated by the current up to 8 A. The sample temperature, controlled by chromel–alumel or Pt–Pt/Rh thermocouples, was determined using the calibration curve $T=f(I)$ computed from standard melting points (http://twt.mpei.ac.ru/PVHB/index.html; http://www2.fkf.mpg.de/xray/html/temperature_calibration. html).

Photo and video filming of domain structures was conducted with a DCM35 digital camera and data images were treated by the ScopeTek ScopePhotoV.3.0 program (http://www.scopetek.com/CameraDevices/index.html).

3. Results and discussion

3.1. Crystal structure determination

The crystal structure of the low-temperature $K_2Sr(MoO_4)_2$ phase was solved in the sp. gr. $C2/c$ based on the observed reflection conditions, and the symmetry was further confirmed in the subsequent structure refinement. The model obtained was refined isotropically with the experimental weighing scheme to $R=0.046$. Attempts to apply the correction for twinning or, more precisely, "tripling" of the crystal showed that it could be neglected since the relative contributions of the minor components were no more than 0.01%. The anisotropic refinement of the structure model resulted in $R=0.0230$, and applying the correction for the secondary extinction and mutual isomorphism of the atoms at the K and Sr sites at the final refinement stage resulted in $R=0.0219$. Crystal and X-ray diffraction data for α-$K_2Sr(MoO_4)_2$ are summarized in Table 1, and atomic coordinates, equivalent isotropic displacement parameters and selected interatomic distances are listed in Tables 2 and 3. The atomic coordinates, anisotropic atomic displacement parameters, and comprehensive data on the crystal structure investigation can be obtained from the Fachinformationszentrum Karlsruhe, 76344 Eggenstein-Leopoldshafen, Germany, (fax: (+49)7247-808-666; e-mail: crysdata@fiz.karlsruhe.de, http://www.fiz-karlsruhe.de/request) on quoting the depository number CSD 425854 for α-$K_2Sr(MoO_4)_2$.

An ORTEP plot of the fragment of the crystal structure fragment of α-$K_2Sr(MoO_4)_2$ is shown in Fig. 1a. Of 7 basic atoms in the structure, only $M1$ is on a twofold axis, the remaining atoms are in general positions. K and Sr atoms are located in the $M1$ and $M2$

Table 1
Crystal data and structure refinement details for α-$K_2Sr(MoO_4)_2$.

Formula weight, g mol^{-1}	485.69
Temperature, K	296(2)
Crystal system, space group	Monoclinic, $C2/c$
Unit cell dimensions	$a=14.318(3)$ Å, $b=5.9337(12)$ Å, $c=10.422(2)$ Å $\beta=105.83(3)°$
Unit cell volume (Å^3)/Z	851.9(3)/4
Calculated density, g cm^{-3}	3.787
$\mu(MoK_\alpha)$, mm^{-1}	10.123
Crystal size, mm^3	$0.12\times0.10\times0.07$
θ range (deg) for data collection	2.96–36.35
Miller index ranges	$-23\le h\le 22$, $-9\le k\le 6$, $-10\le l\le 17$
Reflections collected/unique	5137/2023 [R(int)=0.0211]
No. of variables	63
Extinction coefficient	0.00458(19)
Goodness-of-fit on F^2 (GOF)	1.085
$R(F)$ for $I>2\sigma(I)$	0.0219
$wR(F^2)$ for $I>2\sigma(I)$	0.0534
$R(F)$ for all data	0.0254
$wR(F^2)$ for all data	0.0548
Largest difference peak/hole (e Å^{-3})	1.040/−0.916

Table 2
Atomic coordinates and equivalent isotropic displacement parameters for α-$K_2Sr(MoO_4)_2$ structure.

Атом	*x*/*a*	*y*/*b*	*z*/*c*	U_{eq} (Å^2)*
*M*1**	0	0.31285(5)	0.25	0.01696(7)
*M*2***	0.29136(3)	0.23825(8)	0.35079(4)	0.02308(10)
Mo	0.39905(1)	0.26613(3)	0.04724(1)	0.01334(6)
O1	0.5218(1)	0.1970(3)	0.1093(1)	0.0341(4)
O2	0.3370(1)	0.0511(3)	0.1066(2)	0.0282(3)
O3	0.3672(1)	0.2643(3)	−0.1287(2)	0.0283(3)
O4	0.3769(1)	0.5350(3)	0.1055(2)	0.0291(3)

* $U_{eq}=(U_{11}+U_{22}\sin^2\beta+U_{33}+2U_{13}\cos\beta)/3\sin^2\beta$.
** *M*1 contains 82.7% Sr and 17.3% K.
*** *M*2 contains 8.7% Sr and 91.3% K.

Table 3
Selected interatomic distances (Å) for α-$K_2Sr(MoO_4)_2$ structure.

Mo-tetrahedron			
Mo1–O1	1.747(2)	*M*2-polyhedron	
Mo1–O2	1.761(2)	*M*2–O1d	2.605(2)
Mo1–O3	1.764(2)	*M*2–O2e	2.732(2)
Mo1–O4	1.767(2)	*M*2–O3b	2.766(2)
< Mo1–O >	1.760	*M*2–O4f	2.839(2)
		*M*2–O4g	2.930(2)
*M*1-polyhedron		*M*2–O2	3.007(2)
*M*1–O4a × 2	2.578(2)	*M*2–O2h	3.088(2)
*M*1–O3b × 2	2.595(2)	*M*2–O3g	3.132(2)
*M*1–O1c × 2	2.774(2)	*M*2–O3h	3.161(2)
*M*1–O2c × 2	2.789(2)	*M*2–O4	3.583(2)
< *M*1–O >	2.684	< *M*2–O >	2.984

Symmetry codes: (a) $x-1/2, y-1/2, z$; (b) $-x+1/2, -y+1/2, -z$; (c) $x-1/2, y+1/2, z$; (d) $-x+1, y, -z+1/2$; (e) $-x+1/2, y+1/2, -z+1/2$; (f) $-x+1/2, y-1/2, -z+1/2$; (g) $x, -y+1, z+1/2$; (h) $x, -y, z+1/2$.

positions with preferred localization of Sr (82.7%) in *M*1 and K (91.3%) in *M*2. The Mo atom has tetrahedral coordination with the Mo–O bond lengths of 1.747(2)–1.767(2) Å. The *M*1 atom has CN=8 and the coordination environment is a slightly distorted tetragonal antiprism with the distances *M*1–O 2.578(2)–2.789 (2) Å. The *M*2 atom has a highly irregular coordination with CN=9+1 and *M*2 – O 2.605(2) – 3.161(2) + 3.583(2) Å, which can be described as a rather distorted monocapped tetragonal antiprism with an extra vertex.

MoO_4 tetrahedra share vertices and edges with *M*1 and *M*2 polyhedra. The *M*1 polyhedra are mutually isolated, while the *M*2 polyhedra share their vertices or faces, and *M*1 and *M*2 are linked by faces. As shown in Fig. 1b, the structure of α-$K_2Sr(MoO_4)_2$ is divided into layers parallel to the (100) plane with alternating *M*1 and *M*2 polyhedra.

The structure of the monoclinic α-$K_2Sr(MoO_4)_2$ is closely related to that of the trigonal palmierite, the unit cell vectors are the same as for α-$Pb_3(PO_4)_2$ [7]: $\boldsymbol{a}_m=(-2\boldsymbol{a}_t-\boldsymbol{b}_t+2\boldsymbol{c}_t)/3$; $\boldsymbol{b}_m=-\boldsymbol{b}_t$; $\boldsymbol{c}_m=2\boldsymbol{a}_t+\boldsymbol{b}_t$, where $\boldsymbol{a}_m$, $\boldsymbol{b}_m$, $\boldsymbol{c}_m$, and $\boldsymbol{a}_t$, $\boldsymbol{b}_t$, $\boldsymbol{c}_t$ are vectors of the monoclinic and trigonal unit cells, respectively. According to these relations, the pseudo-trigonal rhombohedral cell parameters of α-$K_2Sr(MoO_4)_2$ are $a_t=5.996$, $b_t=5.934$, $c_t=20.673$ Å; $\alpha=90$, $\beta=91.56$, and $\gamma=119.65°$. The pseudo-threefold axis is perpendicular to the (100) plane which, in turn, is parallel to the plane of the lamellar crystals of α-$K_2Sr(MoO_4)_2$. The pseudo-trigonal character of the structure is revealed in the projections on this plane (Fig. 2a and b) with the observed noticeable deviations from the trigonal symmetry resulting from the shifts of K and Sr atoms and rotations of MoO_4 tetrahedra.

The *M*1 atom exhibits a maximum shift of 0.37 Å from the pseudo-threefold axis passed through (0, ¼, ¼) [7]. The O2 and O4

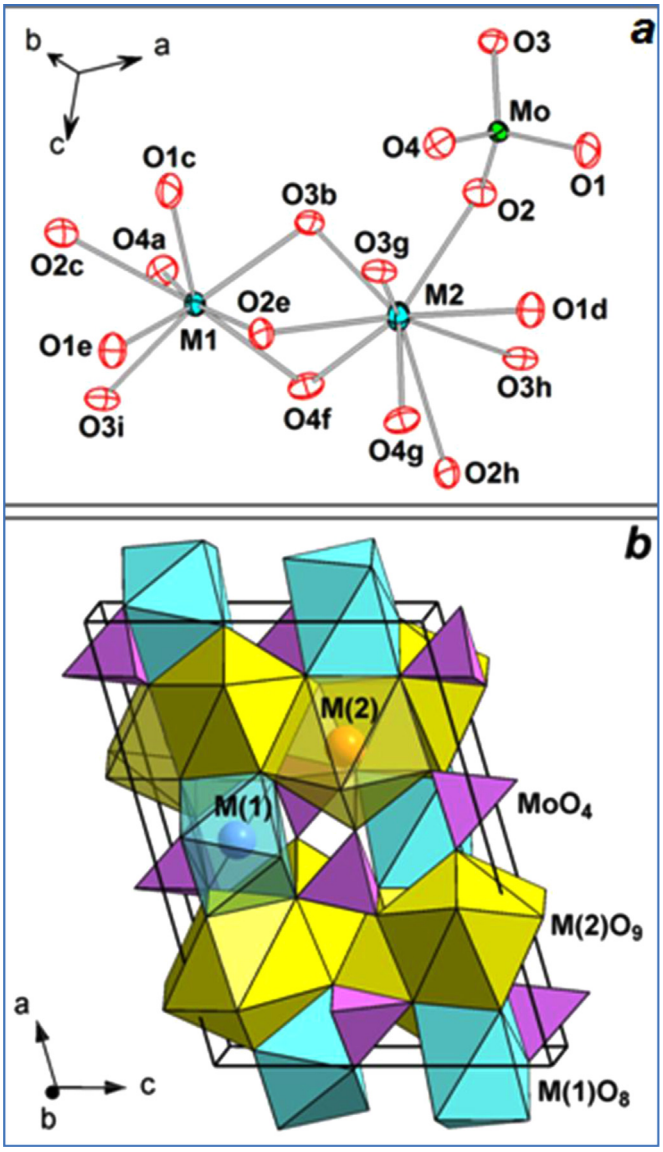

Fig. 1. Structure of α-$K_2Sr(MoO_4)_2$: (a) the asymmetric unit; atomic displacement ellipsoids are shown at 50% probability level. Symmetry codes correspond to those given in Table 3, the additional code: (i) $x-1/2, -y+1/2, z+1/2$. (b) a general view of the structure.

atoms exhibit comparable and even larger displacements from their positions in the "ideal" trigonal structure of 0.37 Å and 0.40 Å, respectively. As a result of atom shifts from the initial positions, the coordination numbers of $M1O_8$ and $M2O_9$ polyhedra change for 6+6 and 10 for Pb and K atoms respectively.

The layered character of the α-$K_2Sr(MoO_4)_2$ structure also fits the palmierite type. One of the layers is composed of separate tetragonal $M1O_8$ antiprisms sharing vertices and edges with MoO_4 tetrahedra (Fig. 2a). Those layers alternate with double layers of the face-shared monocapped tetragonal antiprisms $M2O_9$ with the "inserted" MoO_4 tetrahedra (Fig. 2b).

Although the α-$K_2Sr(MoO_4)_2$ and α-$Pb_3(PO_4)_2$ structures are similarly distorted palmierites and have the same space group [6, 7] they are not completely isostructural because of noticeable differences in atomic shifts and coordinations of the large K^+, Sr^{2+} and Pb^{2+} cations. For example, the *M*2 in the former structure is displaced 0.53 Å from the Pb2 in the latter, while the O4 atoms in the corresponding structures are 0.48 Å apart.

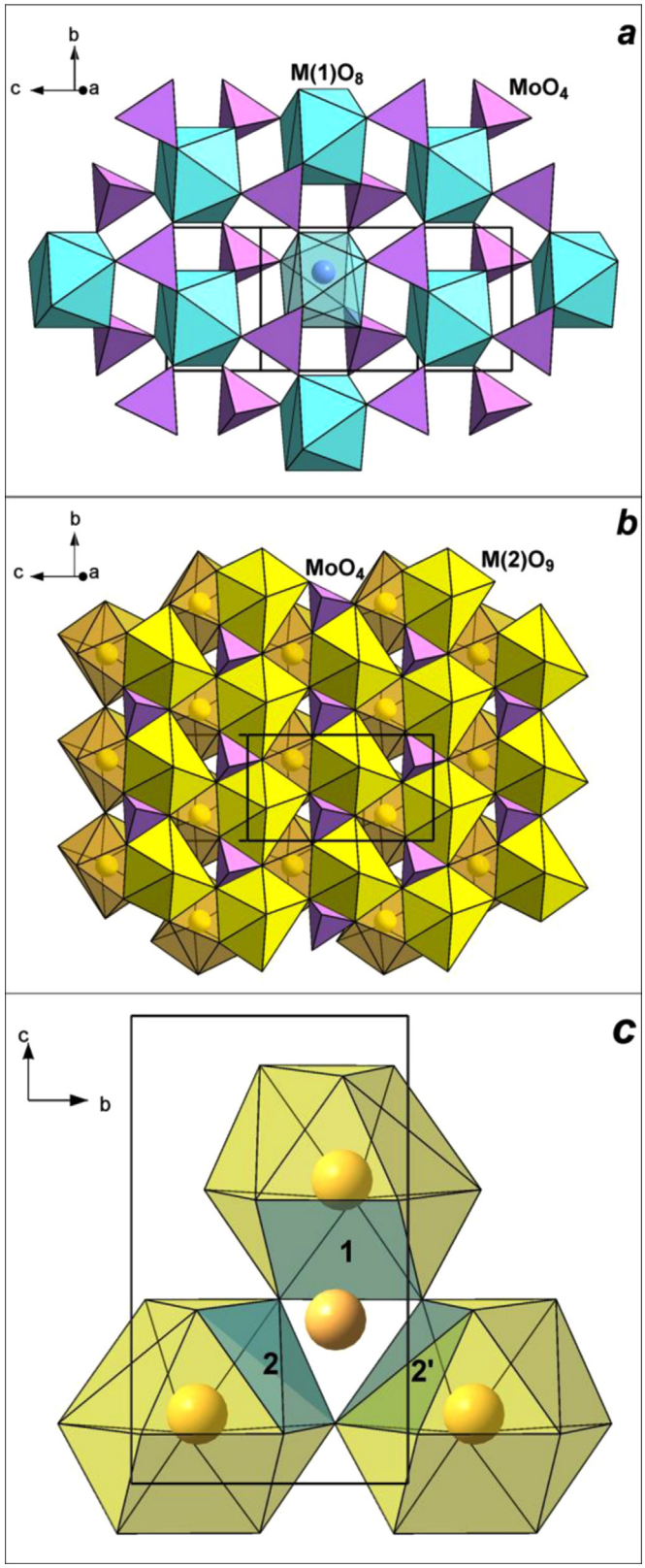

Fig. 2. Fragments of α-$K_2Sr(MoO_4)_2$ structure: a) a layer of $M1O_8$ polyhedra and MoO_4 tetrahedra at $x \approx 0$ projected to the (100) plane; b) a double layer of $M2O_{10}$ polyhedra and MoO_4 tetrahedra at $x \approx 0.25$ projected to the (100) plane (the top and bottom layers are shown with solid and transparent polyhedra, respectively); c) three adjacent $M2O_{10}$ polyhedra surrounding a single $M2$ position (quadrilateral "windows" for potassium ion transportation are marked with integers).

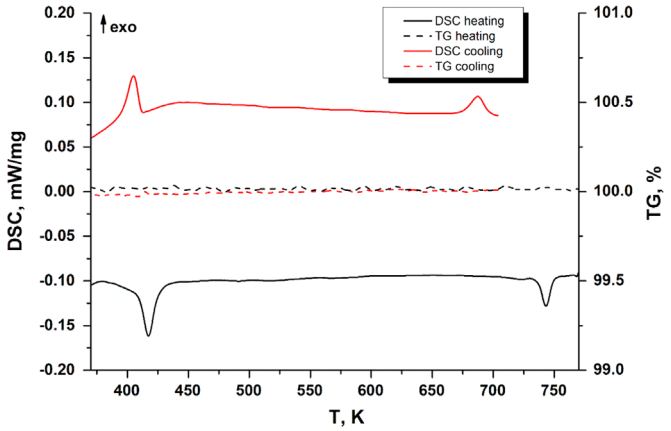

Fig. 3. Heating and cooling DSC and TG curve of a sintered $K_2Sr(MoO_4)_2$ sample (heating rate 10 K min^{-1}).

In α-$Pb_3(PO_4)_2$, Pb1 atom has CN=6+4 with the variation in the distances Pb1–O 2.61 – 2.75 + 3.00 – 3.14 Å [7], whereas in α-$K_2Sr(MoO_4)_2$, the corresponding $M1$ atom is located in a much more isometric 8-vertex polyhedron. Similar irregular coordination typical of Pb^{2+} with CN=10 is observed for Pb2 with the bond distances Pb2–O 2.33–3.38 Å [7], while the $M2$–O distances in the (9+1)-vertex polyhedron around $M2$ are larger in accordance with a larger ionic radius of K^+. The difference between the α-$K_2Sr(MoO_4)_2$ and α-$Pb_3(PO_4)_2$ structures may be attributed to both the differences in stereochemical properties of K^+, Sr^{2+}, Pb^{2+} cations and PO_4^{3-}, MoO_4^{2-} anions and to the differences in values and directions of the atomic shifts under distortions of the trigonal palmierite-like structure of the paraphases.

3.2. *Thermal analysis, crystal optical observations, XRD and phase transitions*

According to DTA data, $K_2Sr(MoO_4)_2$ melts incongruently at 1173 K. A DSC curve (Fig. 3) shows two distinct endothermal effects at T_1=421 K and T_2=744 K corresponding to polymorphic first-order transitions α (LT)→ β (MT)→γ (HT). These phase transitions were also confirmed by the crystal optical observations and videos obtained on a polarizing microscope with a hot stage. All these methods together allow studying of the domain structure and phase transition dynamics of the crystal in dependence of temperature and time. In addition, the point symmetry of the phases may be determined from conoscopic figures [15].

At room temperature in thin colorless plate crystals $K_2Sr(MoO_4)_2$ antiphase domains with sloping walls W' (Fig. 4a) are detected which are characteristic for ferroelastic type 3mF2/m. Domain structure in the crystal is born in the form of thin V-shaped needle-like tip with subsequent and movement of the cross-domain boundary (Fig. 4b). Fig. 4c shows typical domain structures which are extinguished in turn by rotating a polarizing microscope stage through +30°. Large domains disappear as the temperature reaches T_1; above 421 K small domains are formed that become weakly sensitive to the external electric field. At constant temperature, domain wall movement may also be observed upon weak mechanical action on $K_2Sr(MoO_4)_2$ crystal.

According to the Curie principle [16], the geometry of the domain structure occurring at the appropriate phase transition is not arbitrary and is determined by the symmetry elements disappearing after the phase transition. The domains form the macroscopic groups there by imitating the symmetry elements (the three-fold axis in this case, Fig. 4d) which disappeared after the phase transition on cooling.

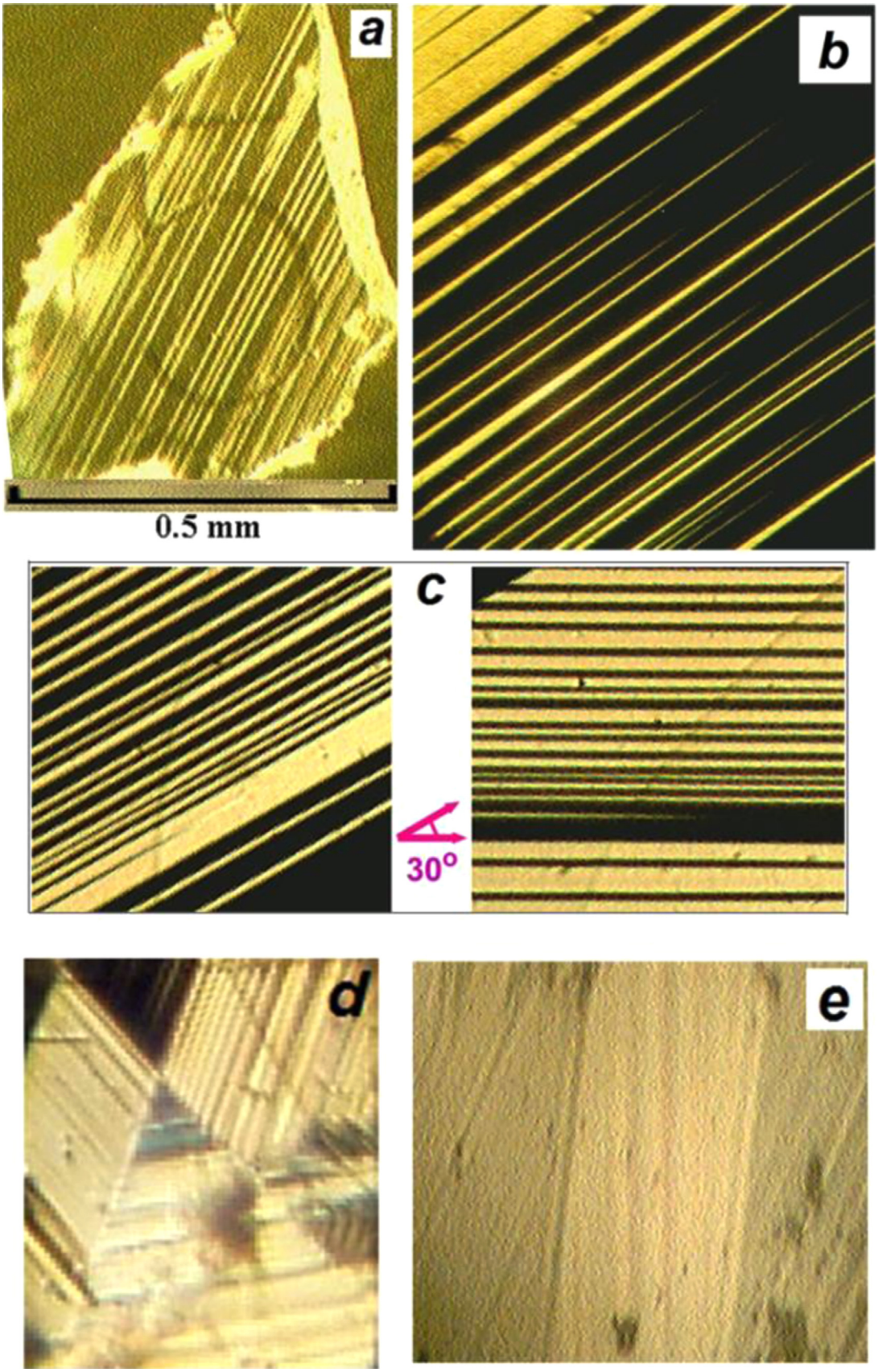

Fig. 4. Ferroelastic α-$K_2Sr(MoO_4)_2$ crystal viewed in polarized light under optical microscoope: (a) general view; (b) ferroelastic domain walls with needle-like tips; (c) domain walls at positions of crystal at 0 and 30°; (d) domain grid with average distance between parallel walls of domains 1–10 μm; (e) slanting domains along the two-fold axis.

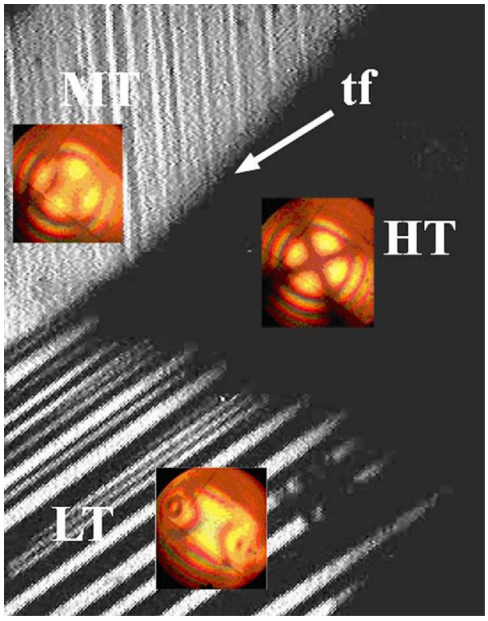

Fig. 5. Change of conoscopic figures of $K_2Sr(MoO_4)_2$ crystal in the course of transition from paraphase (HT, 750 K) to intermediate (MT, 430 K) and to low-temperature ferroelastic phase (LT, 300 K). Thermal front is denoted as tf.

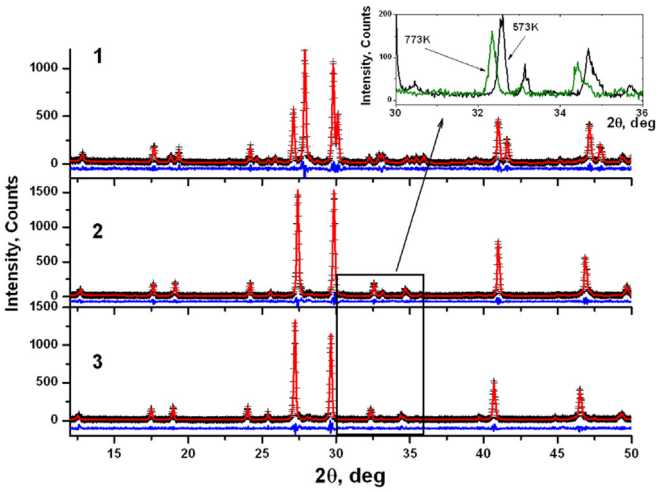

Fig. 6. Powder XRD patterns for $K_2Sr(MoO_4)_2$ at: (1) T=298 K; (2) T=573 K; (3) T=773 K. Black is the experimental XRD pattern, solid red is profile refinement result after LeBail fitting, solid blue is the difference curve. In the inset, the profile fragments of 2θ=30–36° at 573 and 773 K are given to show disappearance of extra peaks after high-temperature phase transition.

Study of monoclinic α-$K_2Sr(MoO_4)_2$ crystal along the two-fold axis direction has revealed interlayers with oblique laminated structures (Fig. 4e). Consequently, below Curie temperature (T_c) the crystal is divided into domains with various layered structures. Most likely inhomogeneous internal stress occurs in each interlayer to extend widely over the appropriate layer, that is, the domains really represent macroscopic formations. The phase transition features and point symmetry of $K_2Sr(MoO_4)_2$ phases were studied through the temperature dependences of the optical properties of the crystal along the direction perpendicular to the lamellar crystals in the range 300–973 K. At these temperatures, the crystals are optically negative. The crystals are biaxial in the range 300-421 K (Fig. 5). Slow heating of a lamellar crystal in transmitted polarized light beam allows phase boundary movement to be observed in the sample. It should be noted that the transition from low- to high-temperature phase is a continuous and reversible process (Fig. 5).

The angle between two axes of the optical indicatrix of the monoclinic phase decreases in the range 300-421 K. Our optical observations showed that the crystal is uniaxial above 421 K (Fig. 3, 5). However, the image was eroded between 421 and 744 K, but it became clear above 744 K. Note that images of the MT phase show the presence of both uniaxial and biaxial crystals. The presence of fragments of LT- and HT- phases in a MT phase was previously observed in the incommensurate (β) phase of $K_5Yb(MoO_4)_4$ [17]. β-$K_5Yb(MoO_4)_4$ is actually built from fragments of α- and γ-phases. Similarly, we can assume that β-$K_2Sr(MoO_4)_2$ is built from the α- and γ-phases. XRD patterns of different modifications of $K_2Sr(MoO_4)_2$ supports this idea (Fig. 6).

All lines on the XRD pattern of low temperature α-phase correspond closely to the monoclinic unit cell found in the single crystal data. The diffraction lines of high temperature γ-phase are indexed in a rhombohedral cell corresponding to the undistorted palmierite structure. Calculated and experimental XRD patterns profiles of $K_2Sr(MoO_4)_2$ sample at different temperatures are shown in Fig. 6. The experimental XRD patterns of the β- and γ-modifications are rather similar: there is only one additional reflection at 2θ=30.50° in the XRD pattern of the β-modification compared with that of the γ-modifications. In the inset the XRD pattern fragments are shown for the range of 2θ=30–36° at temperatures of 573 K and 773 K curves, respectively), which demonstrates disappearing extra peaks during β→γ phase transition. The calculated unit cell parameters, space groups and other XRD data for $K_2Sr(MoO_4)_2$ samples at different temperatures are shown in Table 4. Results obtained for low- and high-temperature forms of $K_2Sr(MoO_4)_2$ agree well with the data from the α-$K_2Sr(MoO_4)_2$ structural study, and they also confirm that the γ-$K_2Sr(MoO_4)_2$ structure is of the palmierite type.

Table 4
XRD powder data for $K_2Sr(MoO_4)_2$ forms at different temperatures.

Form, T (K)	α, 300	γ, 773
Space group	$C2/c$	$R\bar{3}m$
$\boldsymbol{a}$, Å	14.320(2)*	6.024(1)
$\boldsymbol{b}$, Å	5.934(1)	–
$\boldsymbol{c}$, Å	10.428(2)	21.038(3)
$\boldsymbol{\beta}$, °	105.9(1)	–
V, Å^3	852.3(1)	661.2(1)
Z	4	3
R_{wp}	16.78	17.93
GOF	1.20	1.13

* The relations to the palmierite-like phase (γ-form): $\boldsymbol{a}_\alpha=(-2\boldsymbol{a}_\gamma-\boldsymbol{b}_\gamma+2\boldsymbol{c}_\gamma)/3$; $\boldsymbol{b}_\alpha=-\boldsymbol{b}_\gamma$; $\boldsymbol{c}_\alpha=2\boldsymbol{a}_\gamma+\boldsymbol{b}_\gamma$.

However, results for medium-temperature β-$K_2Sr(MoO_4)_2$ cannot be considered as precise and conclusive, so for exact solution of the problem of the unit cell parameters and space group for this phase, additional XRD experiment of high resolution is needed. Probably, β-$K_2Sr(MoO_4)_2$ is incommensurate phase, just as β-$K_5Yb(MoO_4)_4$ [17].

3.3. Dielectric permeability, electrical conductivity and SHG measurements

Dielectric data for α-$K_2Sr(MoO_4)_2$ ceramic pellets over the frequency range 1 Hz to 1 MHz show no evidence of the maxima characteristic of ferroelectric transitions (Fig. 7). However, domain structure peculiarities for α-$K_2Sr(MoO_4)_2$ (Fig. 4) may suggest that below 421 K this phase is ferroelastic similar to $K_5Nd(MoO_4)_4$ [18].

According to Aizu's classification [19], ferroelastic phase transition is possible during change of the crystal systems from

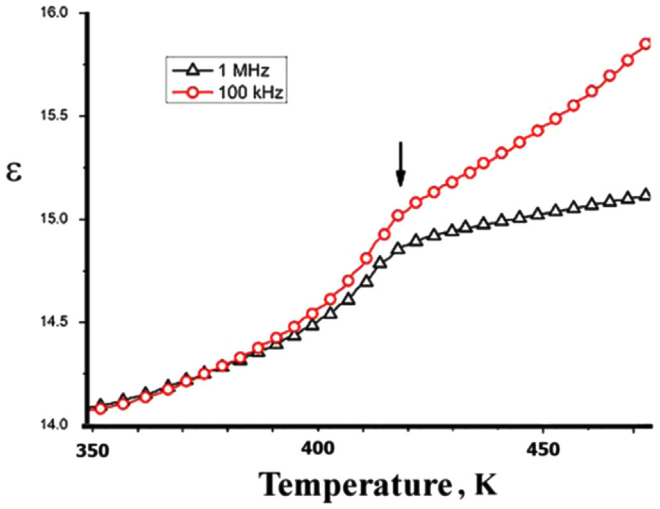

Fig. 7. Temperature dependences of dielectric permittivity (ε) for $K_2Sr(MoO_4)_2$ at different frequencies.

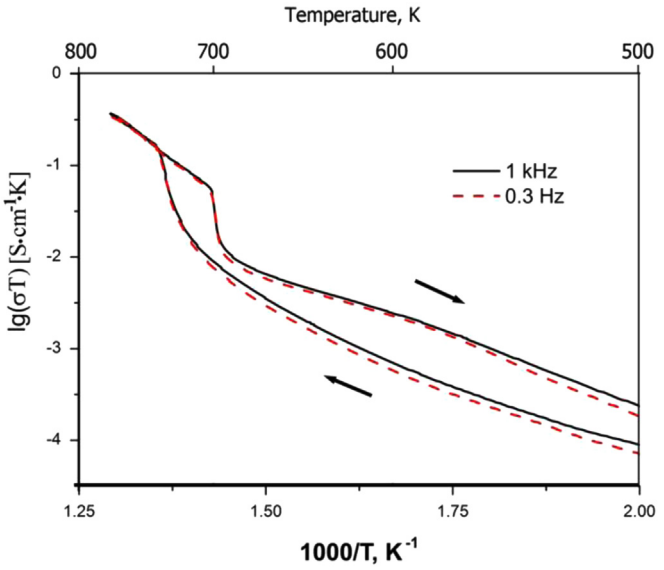

Fig. 8. The dependence of lg (σT) on inverse temperature ($1/T$) for $K_2Sr(MoO_4)_2$ samples at frequencies of 0.3 Hz and 1 kHz during heating and cooling.

trigonal to monoclinic. Analysis of α-, and γ-$K_2Sr(MoO_4)_2$ powdered sample by the SHG method confirms that all these phases are characterized by low SHG signal, $I_{2\omega}/I_{2\omega}(SiO_2) \leq 0.07$, and, therefore, should be considered as centrosymmetric.

The presence of domains in (3×2) orientations shows that paraphase belongs to *m* crystallographic point group [19], which is in a good agreement with high-temperature XRD data.

Distortive-type polymorphic transformation accompanied by changing the number of atoms in the unit cell (i.e. by change of translation vector sets) and crystal point group, according to Indenbom [20] is specific to improper ferroelastic. In this connection, the initial space group should be unequivocally symmorphic. Taking into consideration all the data, it is expected that paraphase of γ-$K_2Sr(MoO_4)_2$ possesses the space group $R\bar{3}m$, $Z=3$ [11] and corresponds to the undistorted palmierite structure. In this case, the crystal point group of ferroelastic phase must be $2/m$, $Z=4$.

Consequently, $K_2Sr(MoO_4)_2$ is an improper ferroelastic at room temperature. The feature for $K_2Sr(MoO_4)_2$ is formation of a regular layer-by-layer structure with domains originating from symmetry lowering of the crystal from trigonal to monoclinic below a distortive phase transition. The results of optical examinations of $K_2Sr(MoO_4)_2$ crystals suggest the sequence of symmetry changes for polymorphic modifications of $K_2Sr(MoO_4)_2$ from paraelectric γ-phase ($R\bar{3}m$) to ferroelastic α-phase ($C2/c$) through an intermediate β-phase with a probable incommensurate structure. In palmierite-like $K_5Nd(MoO_4)_4$, a phase transition was found at 768 K, which being considered by the authors [18] also as ferroelastic. The reason for this is absence of superstructure reflections on Weissenberg photographs, which could lower symmetry from $R\bar{3}m$ to the monoclinic system. However, later on the basis of single crystal data, it was demonstrated that $K_5Nd(MoO_4)_4$ at room temperature is monoclinic [21]. Taking into account this fact and using the data of Maeda [18] we may suppose that ferroelastic phase transitions is a common feature of monoclinic palmierites.

It is interesting that electrical conductivity of $K_2Sr(MoO_4)_2$ increases by a factor of 10 in the vicinity of 744 K (Fig. 8). Due to the absence of frequency dispersion, this effect can be directly assigned to β→γ distortive phase transition at the same temperature, which gives substantially enhanced the potassium ion mobility in the high-temperature phase. From a structural point of view, cationic transport paths in α-$K_2Sr(MoO_4)_2$ should pass through "bottlenecks" as quadrilateral windows of *M*2 coordination polyhedra (Fig. 2c). However, bond valence sums calculated according to http://www.softbv.net for the centroids of the windows are 2.039 v.u. (centrosymmetrical window 1) and 1.652 v.u. (asymmetrical window 2), implying that at room temperature the potassium ions are preferentially transported through windows 2, i.e. a quasi-one-dimensional ionic conductivity along the *b* axis. Obviously, with increasing the crystal symmetry at β→γ distortive transition, the windows 1 and 2 as well as the ionic transport channels become symmetrically uniform in γ-$K_2Sr(MoO_4)_2$ and its ionic conductivity obtains a two-dimensional character.

Taking into consideration that $K_2Sr(MoO_4)_2$ includes only large cations at long distances from each other and relatively narrow "bottlenecks" between their coordination polyhedra, the cation conductivity can not be very large, which is in full agreement with the registered values of 10^{-4}–$10^{-3}\ \Omega^{-1}\ cm^{-1}$ at phase transition temperature of 744 K. Moreover, high activation energy ~1.2 eV points directly to the presence of large charge carrier mobility.

Studies of cation conductivity in single crystals of palmierite-related $K_5R(MoO_4)_4$ (R=Bi, Nd, Gd) [22] also show noticeable mobility of K^+ ions (up to $10^{-3}\ \Omega^{-1}\ cm^{-1}$) in the directions parallel to the structure layers. Ca^{2+} and Sr^{2+} ionic conductivity is also observed in cation-deficient palmierites $Ca_{3-x}La_{2x/3}(VO_4)_2$ ($0.8 \leq x \leq 1$) [23] and $Ca_{2.4}La_{0.4}(V_{1-y}P_yO_4)_2$ ($0 \leq y \leq 1$) [24].

For the three phases of palmierite-related $K_5Yb(MoO_4)_4$ [17], it was observed that the occupations of *M*1 and *M*2 positions change from ordered type to statistical with increasing temperature, indicating the possibility of moving large cations from one position to another. Taking this into account, the transition around 744 K in the structure of $K_2Sr(MoO_4)_2$ into a high conductivity state might be related to further disordering K^+ and Sr^{2+} cations and enhancement of their general mobility.

It is interesting to note that crystal structures of monoclinic low-temperature palmierite-like $K_2Sr(MoO_4)_2$, $K_2Pb(MoO_4)_2$ [9] and $Rb_2Pb(MoO_4)_2$ [10] studied so far have various types of distortions. For example, the unit cell vectors of α-$Rb_2Pb(MoO_4)_2$ ($\boldsymbol{a}$, $\boldsymbol{b}$, $\boldsymbol{c}$) and palmierite ($\boldsymbol{a}_p$, $\boldsymbol{b}_p$, $\boldsymbol{c}_p$) are connected by relationships: $\boldsymbol{a}=2\boldsymbol{a}_p+4\boldsymbol{b}_p$, $\boldsymbol{b}=-2\boldsymbol{a}_p$, $\boldsymbol{c}=2(-\boldsymbol{a}_p-2\boldsymbol{b}_p+\boldsymbol{c}_p)/3$. In its turn, the unit cell of α-$Rb_2Pb(MoO_4)_2$ has a simple connection with the unit cell of α-$K_2Pb(MoO_4)_2$ [6]: $\boldsymbol{a}_{RbPb}=-2\boldsymbol{a}_{KPb}$, $\boldsymbol{b}_{RbPb}=2\boldsymbol{c}_{KPb}$, $\boldsymbol{c}_{RbPb}=2\boldsymbol{b}_{KPb}$, which indicates a complicated structure of the former. Above mentioned examples give evidence, that though high-temperature phases of palmierite family all are trigonal and isostructural, architecture of their low-temperature phases can depend heavily on

their composition. This shows that mechanisms of palmierite structure distortions are distinct in each case, and these mechanisms are probably connected both with the influence of other cations and tetrahedral anions. Our data for the structure of α-$K_2Sr(MoO_4)_2$, one more member of the palmierite family, confirm again that, depending on composition, the structure and properties of these compounds vary in details. Purposeful modification of this information (for example, by isomorphous substitutions) can be used to control the functional properties of double molybdates and other palmierite-related compounds, which can be used as elements of memory or switches.

Acknowledgments

This work was partially supported by the Ministry of Education and Science of the Russian Federation (Grant no. 3.6021.2011) and by the Russian Foundation for Basic Research (Grants RFBR 11-03-90714-mol_rf_nr, nos. 13-03-01020 and 14-03-00298).

References

[1] V. Janovec, J. Přívratska, Int. Tables Crystallogr. D (2006), ch. 3.4.
[2] V.A. Efremov, V.K. Trunov, Crystallogr. Rep. 19 (1974) 989–993.
[3] E.F. Dudnik, G.A. Kiosse, Bull. Acad. Sci. USSR Phys. Ser. 47 (1983) 420–434.
[4] V.K. Trunov, V.A. Efremov, Yu.A. Velikodny, Crystal Chemistry and Properties of Double Molybdates and Tungstates, Nauka: Leningrad, Russia, 1986.
[5] C.K. Møller, Acta Chem. Scand. 8 (1954) 81–87.
[6] U. Keppler, Z. Kristallogr. 132 (1970) 228–235.
[7] D.M.C. Guimaraes, Acta Crystallogr. A35 (1979) 108–114.
[8] E.F. Dudnik, I.E. Mnushkina, Ukr. J. Phys. 22 (1977) 1737–1738.
[9] V.A. Efremov, V.K. Trunov, Bull. Sci. USSR 235 (1977) 820–823.
[10] I.A. Gudkova, Z.A. Solodovnikova, S.F. Solodovnikov, E.S. Zolotova, J. Struct. Chem. 52 (2011) 1063–1071.
[11] V.K. Trunov, Russ. J. Inorg. Chem. 16 (1971) 553–554.
[12] A.A. Coelho, TOPAS Academic: General Profile and Structure Analysis Software for Powder Diffraction Data, Bruker AXS, Karlsruhe, Germany, 2004.
[13] G.M. Sheldrick, Acta Crystallogr. A64 (2008) 112–122.
[14] R.W. Vest, N.M. Tallan, J. Appl. Phys. 36 (1965) 543–548.
[15] N.M. Melanholin, The Methods of the Study Optical Characteristics of Crystals, Science, Moscow, 1970.
[16] J.F. Nye, Physical Properties of Crystals, Clarendon Press, Oxford, 1957.
[17] V.A. Morozov, B.I. Lazoryak, O.I. Lebedev, S. Amelinckx, Van G. Tendeloo, J. Solid State Chem. 176 (2003) 76–87.
[18] M. Maeda, K. Sakiyama, T. Ikeda, Jpn. J. Appl. Phys. 18 (1979) 25–29.
[19] K. Aizu, Phys. Rev. B2 (1970) 754–768.
[20] V.L. Indenbom, Bull. Acad. Sci. USSR Phys. Ser. 43 (1979) 1631–1640.
[21] B.I. Lazoryak, V.A. Efremov, Crystallogr. Rep. 31 (1986) 237–243.
[22] V. Trnovcová, A. Škubla, D. Schulze, Solid State Ion. 176 (2005) 1739–1742.
[23] I.A. Leonidov, O.N. Leonidova, L.L. Surat, R.F. Samigullina, Inorg. Mater. 39 (2003) 616–621.
[24] O.N. Leonidova, E.I. Leonidova, Solid State Ion. 179 (2009) 188–191.